NUMERICAL INVESTIGATION OF VORTEX-INDUCED VIBRATION OF A VERTICAL RISER IN UNIFORM FLOW AT HIGH REYNOLDS NUMBERS

Jerónimo Domingo
Escuela Técnica Superior de Ingenieros Navales, Universidad Politécnica de Madrid (UPM), Avenida Arco de la Memoria, 4, 28040, Madrid, Spain., jeronimo.domingo.guijarro@alumnos.upm.es

Luis Pérez-Rojas
Escuela Técnica Superior de Ingenieros Navales, Universidad Politécnica de Madrid (UPM), Avenida Arco de la Memoria, 4, 28040, Madrid, Spain.

H. R. Díaz-Ojeda
Escuela Técnica Superior de Ingenieros Navales, Universidad Politécnica de Madrid (UPM), Avenida Arco de la Memoria, 4, 28040, Madrid, Spain.

NUMERICAL INVESTIGATION OF VORTEX-INDUCED VIBRATION OF A VERTICAL RISER IN UNIFORM FLOW AT HIGH REYNOLDS NUMBERS

Jerónimo Domingo[1], Luis Pérez-Rojas[1] and H. R. Díaz-Ojeda[1]

ABSTRACT

This work presents a numerical study on the vortex-induced vibration (VIV) phenomenon of synchronization of a vertical, flexible, circular cylinder with a length-to-diameter ratio of 475, being free to move along the in-line (IL) and cross-flow (CF) directions for Reynolds numbers of 42K, 84K and 126K. It is found that the dominant mode numbers, the maximum root mean square amplitudes, the dominant frequencies and the lift coefficient increase with the Reynolds number, but the drag coefficient decreases. The in-line response shows a main frequency component at twice the cross-flow frequency. At some Reynolds number value and riser span location, a third harmonic frequency component is observed in the CF response.

The aims of this paper are to study the lock-in phenomenon and the effect of the flow-induced tension in the riser frequency spectrum. The lock-in analysis shows that when both the cross-flow riser movement and the velocity transversal component frequency values are the same, lock-in takes place. The lock-in is established at the vibration mode predominant frequency for the three Reynolds numbers.

The results show also that, taking into account the tension produced by the flow, the vibration frequency spectrum will be calculated accurately. The drag force produces a flow-induced tension that makes the riser behave as a tension-dominated riser, even if the riser was not pre-tensioned.

I. INTRODUCTION

Vortex-induced vibration (VIV) of slender structures is of practical interest in many fields of engineering. VIV often causes fatigue of onshore and offshore structures, such as risers, mooring lines, tension legs, etc. Detailed understanding of this fluid-structure interaction (FSI) phenomenon, as well as an efficient prediction of such self-excited and self-sustained oscillations, are required for the reliable estimation of the fatigue damage and the development of VIV suppression techniques (Bourghet et al., 2011a, 2013).

VIV has been extensively studied. Comprehensive, state-of-the-art reviews were published by Sarpkaya (1979), Bearman (1984), Williamson and Govardhan (2004), Gabbai and Benaroya (2005), Bearman (2011) and Wu et al. (2012). As these types of structures often have a length-to-diameter ratio (L/D) of the order of $10^2 - 10^3$ (Meneguini et al., 2004; Chaplin et al., 2005; Resvanis et al., 2012), several experiments have been carried out on deepwater risers with large L/D (Tognarelli et al., 2004; Chaplin et al., 2005; Trim et al., 2005; Lie and Kaasen, 2006; Vandiver et al., 2006; Tognarelli et al., 2008; Vandiver et al., 2009; Huang et al., 2011b; Resvanis et al., 2012; Gu et al., 2013; Gao et al., 2015). These experiments investigated flexible riser's VIV response under different flow conditions, and some also addressed the effectiveness of VIV suppression techniques, such as using helical strakes. These are all the tests recently used as validation source for the numerical studies.

Our experimental investigations were carried out at different towing tanks having their own limitations in terms of riser length and carriage velocity maximum speed. To avoid length limitation, Chaplin et al. (2005) located an important part of the riser inside a tube at vacuum conditions that moved with the carriage, with this part of the riser having zero velocity. This type of velocity profile is named as stepped, and in this case had a non-zero velocity in its lower 5.9 m: the towing tank's depth. The maximum Reynolds number achieved was approximately 28K.

Trim et al. (2005) investigated a 38 m long, 27 mm diameter riser fixed in a horizontal facility that was set in a longitudinal towing tank to investigate uniform flow response, and in a

Table 1. Nomenclature of used variables.

Nomenclature			
A_{xrms}/D, A_{yrms}/S	Dimensionless in-line and cross-flow root mean square amplitudes	IL	Acronym of in-Line (flow direction)
A_{xrms}^{max}/D, A_{yrms}^{max}/D	Dimensionless maximum root means square amplitudes	$m^* = m/\left(\rho\pi D^2 4\right)$	Mass ratio
C	Structural damping	N	Mode number
C_D	Drag coefficient	R	Riser radius (in m)
CF	Acronym of Cross Flow (direction perpendicular to flow).	Re	Reynolds number
C_L	Lift coefficient	S	Surface
c_m	Added mass constant	S_t	Strouhal Number
D	Riser outer diameter (in m)	T	Instant time
E	Young Modulus	T	Tension
EI	Flexural rigidity (product of Young modulus and inertia moment)	V	Uniform flow velocity
F	Force	X	In-line displacement
f_n	Natural frequency of the oscillating mode (in Hz)	x_{mean}	Mean in-line displacement
$f_{n,beam}$	.nth natural frequency for a non-tensioned beam (in Hz)	Y	cross-flow displacement
$f_{n,string}$	.nth natural frequency for a tensioned string (in Hz)	ε	Strain
I	Inertia moment	σ	Stress
K	Wavenumber	ρ	Water density
L	Riser length (in m)	ν	Water kinematic viscosity
M	Mass	ω_c, ω_b	Cable and beam phase velocities.
m_a	Added mass		

rotating towing tank to investigate sheared flow response. Riser behavior differences in uniform and sheared flows were investigated, and reached Reynolds numbers near 65K.

Lie and Kaasen (2006) investigated a much longer riser, up to 90 m, by using a special facility off the coast of Norway near Bergen. The installation consists of a 180 m long floating quay at 97 m sea depth. The riser model was attached to a floating vessel that was moved along the quay side by a rope and engine system. The other riser´s extreme was fixed at the sea bottom. By moving the vessel at constant velocity, the riser was exposed to a triangular current velocity profile or sheared flow. The maximum Reynolds number was approximately 35K. The effect of very high riser length to diameter ratios was analyzed.

Tognarelli et al. (2008) used a 10 m long riser located in a rotating rig facility, and perpendicular to rotating facility axis. Hence, the riser local span velocity increases linearly with its distance to the rotating axis, producing a so-called sheared flow. The tests analyzed the effect of a non-uniform velocity on the riser´s behavior. The maximum Reynolds number was near 70K.

Resvanis et al. (2012) also investigated the 38 m long riser in the same installation as Trim et al. (2005), but with three different riser diameters: currently 12, 30 and 80 mm. This last riser diameter was achieved by surrounding the 30 mm riser with a 25 mm thick plastic shell. Reynolds numbers ranged from 42K to 126K for uniform flows. Correlations of in-Line (IL), and cross-flow (CF), oscillation amplitudes as

functions of Reynolds numbers reaching the highest Reynolds number range in towing tank tests were obtained.

Better understanding of some important VIV aspects (i.e. response amplitude, dominant mode, dominant frequency, fatigue damage, etc.) were obtained from the above mentioned experimental works. Furthermore, they provided the benchmarks for verifying numerical prediction models. Nevertheless, in all of these experimental works the Reynolds numbers yielded in the low Reynolds number range due to the test facilities´ limitations. But, according to Trim et al. (2005): "For a full-scale riser diameter of (say) 0.5 m and ocean currents up to 2 m/s, Reynolds numbers approaching the millions may apply, embracing three flow regimes: subcritical, critical and supercritical". This makes analyzing high Reynolds VIV an important task.

The most important phenomena of VIV at high Reynolds are that both the forces and the oscillation amplitudes experienced by the riser will be larger (Resvanis et al., 2012), and hence, also tensions and reactions at their extremes. These are basic parameters for riser design. On the other hand, the vortex shedding also varies with the Reynolds number. The accurate determination of the vortex shedding frequency spectrum for high Reynolds numbers is required, as it will be compared to the riser structure frequency spectrum to check the occurrence of lock-in, the most dangerous condition to produce riser damage by fatigue. The lock-in phenomenon occurs when both vortex shedding and structure frequency values are equal. Finally, the structure frequency spectrum

depends on riser tension which, at the same time, depends on the forces produced by the flow upon the cylinder. In this way, the structure frequency value will also vary for high Reynolds numbers.

Besides the experimental investigations, the other research methodology on flexible cylinders' VIV has been Computational Fluid Dynamics (CFD). As will be observed next, all of them have concentrated again into low Reynolds numbers.

Newman and Karniadakis (1997) carried out VIV a simulation of an infinitely long flexible cable at Re = 100 and Re = 200 with a spectral/hp element method. Both the standing wave and the traveling wave responses were realized. It was found that the interwoven pattern of vorticity was associated with a standing wave cable response.

Holmes et al. (2006) and Menter et al. (2006) introduced commercial software codes to analyze VIV. They used two different approaches to investigate riser VIV: the fully 3D Finite Element Method (FEM) and the Finite Volume Method (FVM). Both simulations used relatively coarse meshes with high element aspect ratios, and their results for vibration modes and maximum oscillation amplitudes were in good agreement with the experimental data by Trim et al. (2005) and Chaplin et al. (2005).

Bourghet et al. (2011a, 2011b, 2012, 2013 and 2015) did a series of fundamental studies on the VIV of flexible cylinders. Their research revealed some important flexible cylinder VIV mechanisms such as the occurrence of lock-in, the orbital trajectories which dominate the wake-body resonance, the phasing mechanisms between the IL and CF VIV and the validity of the independence principle (IP) applied to VIV.

Lothode et al. (2015) analyzed a 1 m diameter 2D fixed cylinder at Reynolds numbers 43K and 71K and the riser of the Chaplin et al. (2005) tests at Reynolds number 4.5K. They obtain good accuracy in the vibration mode shape and acceptable accuracy in the amplitudes.

Xiao and Wang (2016) simulated combined IL and CF VIV of a 9.53 m long vertical riser in uniform and linearly sheared currents using a fully 3D CFD approach. The Reynolds numbers are approximately 2K and 4K. Oscillation envelopes and amplitudes were in good agreement with the test results.

Nevertheless, fully 3D FSI simulations of VIV of a vertical riser subjected to various flow conditions are still quite limited. Past studies found that the dominant modes were related to the incoming flow velocity profile (Huang et al., 2011a), and the IL VIV should not be neglected in deepwater riser design (Tognarelli et al., 2004; Xue et al., 2015).

The aim of this work is to analyze much higher Reynolds numbers, in the range of 42K to 126K. To do so, a riser with similar length to diameter ratios, Young modulus, mass ratio and inertia moment to those found in the bibliography has been chosen. This riser will be immersed in flows of three different velocity values: values that produce Reynolds numbers of 42K, 84K and 126K. From each case the envelopes, the oscillation time histories and the oscillation frequencies in both the In-Line (IL) and Cross-Flow (CF) directions will be analyzed. The appearance of synchronization, or lock-in, will be analyzed. Orbital trajectories will be found. Finally, how accurately riser frequency spectra can be calculated will be assessed, taking into account the tension produced by flow induced riser deformation.

II. NUMERICAL METHODS

A commercial software package ANSYS MFX multi-field solver has been adopted to solve the Fluid Structure Interaction (FSI) problem. An FSI problem is one where the flow pattern produces forces upon a body that change its shape. In turn, this change of body shape changes the flow pattern, giving rise to an interaction between the fluid flow and the body structure.

1. Flow model

The flow field around the riser is solved by using the unsteady, incompressible Navier-Stokes equations:

$$\frac{\partial \overline{u}_i}{\partial x_i} = 0 \tag{1}$$

And:

$$\frac{\partial \overline{u}_i}{\partial t} + \overline{u}_j \frac{\partial \overline{u}_i}{\partial x_j} = -\frac{1}{\rho}\frac{\partial \overline{p}}{\partial x_i} + \frac{\partial}{\partial x_j}\left[\nu\left(\frac{\partial \overline{u}_i}{\partial x_j} + \frac{\partial \overline{u}_j}{x \partial_i}\right)\right] - \frac{\partial \tau_{ij}}{\partial x_j} \tag{2}$$

Where $(x_1, x_2, x_3) = (x,y,z)$ are the Cartesian coordinates, the overbar denotes that the variable is a filtered variable, u_i is the velocity component in the x_i direction, p is the pressure, t is the time, ρ is the fluid density, ν is the kinematic viscosity of the fluid and τ_{ij} is the subgrid-scale stress defined as:

$$\tau_{ij} = \overline{u_i u_j} - \overline{u}_i \overline{u}_j \tag{3}$$

Based on the Boussinesq approximation:

$$-(\tau_{ij} - \frac{\delta_{ij}}{3}\tau_{kk}) = 2\nu \overline{S}_{ij} \tag{4}$$

The governing equations are discretised using an element-based Finite Volume Method (FVM). As turbulence model, the SST (Shear Stress Transport) k-ω model of Menter (1994) has been chosen. This model has been widely tested for cases where accuracy is required both in the boundary layer, Menter et al. (2006), Lothode et al. (2015), where the model becomes the k-ω model; and also far from the boundary layer, where the model becomes the k-ε model:

$$\frac{\partial(\rho k)}{\partial t} + \frac{\partial(\rho u_i k)}{\partial x_i} = \frac{\partial}{\partial x_i}\left[\left(\mu + \frac{\mu_t}{\sigma_k}\right)\frac{\partial k}{\partial x_j}\right] + P_k - \rho\varepsilon \tag{5}$$
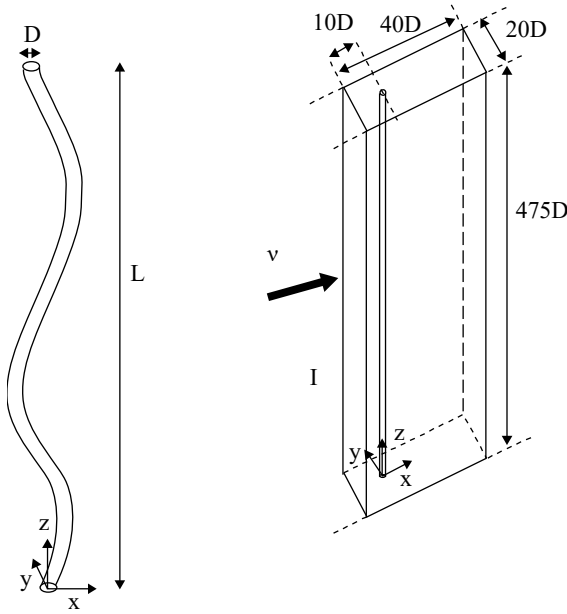
Fig.1. Scheme of the riser (left) and the simulation domain (right) with the riser immersed in the fluid domain.

$$\frac{\partial(\rho\varepsilon)}{\partial t} + \frac{\partial(\rho u_i \varepsilon)}{\partial x_i} = \frac{\partial}{\partial x_i}\left[\left(\mu + \frac{\mu_t}{\sigma_k}\right)\frac{\partial\varepsilon}{\partial x_j}\right] + \frac{\varepsilon}{k}(C_{\varepsilon 1}P_k - C_{\varepsilon 2}\rho\varepsilon) \quad (6)$$

Where P_k is the turbulence production due to viscous and buoyancy forces:

$$P_k = \mu_t \frac{\partial u_i}{\partial x_i}\left[\frac{\partial u_i}{\partial x_j} + \frac{\partial u_j}{\partial x_i}\right] - \frac{2}{3}\frac{\partial u_i}{\partial x_j}\left(3\mu_t \frac{\partial u_i}{\partial x_i} + \rho k\right) + P_{kb} \quad (7)$$

And where $C_{\varepsilon 1}$, $C_{\varepsilon 2}$, σ_k are model constants.

The simulations run with a high-resolution advection scheme, a second order backward Euler for the transient scheme, a high resolution for the turbulence numerics and a convergence criterion of 1e-4.

The convenience of including a model for the local flow transition from laminar to turbulent has been considered. But, according to software code handbook, in this case its inclusion is not recommendable, due to the Reynolds number range and the riser to be moving. The model is convenient for fixed cylinders.

2. Structural model

The structural model is the standard for a transient analysis of a solid piece. This model consists of the use of block type elements. The numerical model is that of an iterative process where the element stiffness matrix with the boundary condition of fixed ends and a pressure field upon its lateral surface is solved for each time step. The pressure field is calculated in the fluid-dynamic part of the FSI model. The solution for a given time step is used as an initial estimator of the next one.

According to Huang et al. (2011a) and Jhingran et al. (2008), the equation of a riser can be taken as that of a tensioned beam, whose flow direction (IL) and lateral motion (CF) are described, respectively, as:

$$\frac{\partial^2}{\partial z^2}\left[EI\frac{\partial^2 x}{\partial z^2}\right] - \frac{\partial}{\partial z}\left[T\frac{\partial x}{\partial z}\right] + (m(z) + m_a(z))\frac{\partial^2 x}{\partial t^2} + c\frac{\partial x}{\partial t} = F_x \quad (8a)$$

$$\frac{\partial^2}{\partial z^2}\left[EI\frac{\partial^2 y}{\partial z^2}\right] - \frac{\partial}{\partial z}\left[T\frac{\partial y}{\partial z}\right] + (m(z) + m_a(z))\frac{\partial^2 y}{\partial t^2} + c\frac{\partial y}{\partial t} = F_x \quad (8b)$$

EI is named the structural flexibility. E is the Young's modulus and I is the riser section moment of inertia. The moment of inertia has the same value for IL and CF motions as riser section is a circle. T is the riser tension. m is the mass per length unit, m_a the added mass per length unit. The added mass has also the same value for IL and CF motions due to the same reason that in the case of the inertia moment. c is the structural damping, z is the non-deformed riser axial direction, as shown in Fig. 1. x denotes the in-line (IL) direction, y the cross-flow (CF) direction. F_x is the hydrodynamic force in the IL direction, which is formed by both the flow drag force and the periodic vortex shedding force IL component. F_y is the hydrodynamic force in the CF direction, which is the periodic vortex shedding force CF component.

Eq. 8a and b respond to the phenomena of a body immersed in a flow. A body immersed in a fluid that flows at a certain velocity experiences a force upon it in the flow direction. This force is named the drag force and depends on: the body area facing the flow, the body shape, the fluid density and the flow velocity.

If the body is not rigid, as it is in the case of a riser, it reacts to such drag force with a shape deformation and elongation. At the same time, a tension field inside the body arises. The tension and elongation relationship can be calculated with eq. 9.

$$\varepsilon = \frac{\Delta L}{L} = \frac{\sigma}{E} \quad (9)$$

Where $\sigma = T/A$, being T the riser tension and A its section area. L is the riser length and ΔL is the riser elongation.

The tension, together with the body´s structural flexibility, determines the body structural vibration frequency spectrum. This spectrum is given by eq. 10, 11 and 12, Weaver et al. (1974) and Xiao and Wang (2016):

$$f_{n,t-beam} = \sqrt{f_{n,string}^2 + f_{n,beam}^2} \quad (10)$$

Where $n = 1,2,...n$ is the mode number and:

$$f_{n,string} = \frac{n}{2}\sqrt{\frac{T}{mL^2}} \quad (11)$$

Table 2. Riser dimensionless elongation and tension as functions of Reynolds numbers.

Reynolds number	$\Delta L/L$	T [N]
42K	2.92e-5	5080
84K	4.44e-5	7722
126K	5.87e-5	10211

Table 3. Structural frequency spectrum of the present work riser.

		Riser vibration frequency spectra					
n	f_{beam}	f_{string} (Re = 42K)	f_{string} (Re = 84K)	f_{string} (Re = 126K)	f_{total} (Re = 42K)	f_{total} (Re = 84K)	f_{total} (Re = 126K)
1	0.02	0.97	1.19	1.37	0.97	1.19	1.37
2	0.08	1.94	2.39	2.75	1.94	2.39	2.75
3	0.17	2.91	3.58	4.12	2.91	3.59	4.12
4	0.30	3.88	4.78	5.49	3.89	4.79	5.50
5	0.47	4.84	5.97	6.87	4.87	5.99	6.88
6	0.68	5.81	7.17	8.24	5.85	7.20	8.27
7	0.92	6.78	8.36	9.62	6.84	8.41	9.66

And:

$$f_{n,beam} = \frac{n^2 \pi}{2} \sqrt{\frac{EI}{mL^4}} \qquad (12)$$

The need for these three eq. (10 to 12) is due the fact that there is no equation that directly gives the value of the structural frequency spectrum for a tensioned beam. But it was found, Weaver et al. (1974), that this set of values can be calculated as a combination of both the structural frequency of a tensioned string, and of the structural frequency of a non-tensioned beam. In this way, the nth structural frequency of a tensioned beam $f_{n,\ t-beam}$ is a function of the nth structural frequency of a tensioned string $f_{n,string}$, and the nth structural frequency of a non-tensioned beam $f_{n,beam}$. The tensioned string component accounts for the pre-tension to which a cylinder might be subjected directly at its installation. The non-tensioned beam component accounts for the riser material and the geometry characteristics. Riser material is represented by its Young modulus E and cylinder geometry characteristics by their section inertia moment I. Hence, the nth value of the spectrum of a tensioned beam can be found with equation 10, the structural tensioned string frequency component with the eq. 11 and the non-tensioned beam component with eq. 12.

Later on, Vortex-Induced Vibration VIV will take place and superpose on the deformed and elongated riser. Above some certain Reynolds number value, these vibrations appear as if the flow pattern around the body is not constant with time. Beside the constant velocity flow pattern, which produces the drag force, vortices appear from the flow direction perpendicular body extremes. These vortices shed alternatively from one extreme and the other. This characteristic of alternatively shedding from the body extremes is responsible for riser vibration in the following manner: the vortices spreading pro-

duces upon the body surface and alternating pressure field. An alternating force arises as the resultant force of this alternating pressure field. The vortex shedding frequency, and therefore the alternating force frequency, depends on the Reynolds number.

When the vortex shedding frequency equals one of the body frequency spectrum values, the lock-in phenomenon occurs. Lock-in is a self-sustaining vibration, and may represent a high-risk situation for riser integrity.

One of the main aims of the present work is to demonstrate that the body vibration frequency spectrum must be calculated for the deformed and elongated riser, rather than for the riser at rest.

Therefore, the calculation procedure is the following: the simulations are carried out, and the time-averaged riser in-line displacements for each flow velocity are found. These displacements are shown in Fig. 4. By applying Eq. 13 to these time-averaged displacement curves the riser elongations are obtained.

$$L' = \sum_i \sqrt{\left(x_i - x_{i-1}\right)^2 + \left(z_i - z_{i-1}\right)^2} \qquad (13)$$

Being the difference between this calculated length L' and the original riser length L, the riser elongation is ΔL. Next, the riser tension is obtained by entering these elongations into Eq. 9. These elongations and tensions are shown in Table 2. Finally, the tensions are introduced into Eq. 10 to 12 to obtain the riser frequency spectrum for each Reynolds number, represented in Table 3. The correctness of this procedure is checked by obtaining the riser oscillation frequency values from time-story graphics, figs 6 and 7, and summarized in Table 4, and comparing them with the values of Table 3. The accuracy of both sets of values demonstrates the validity of the procedure.
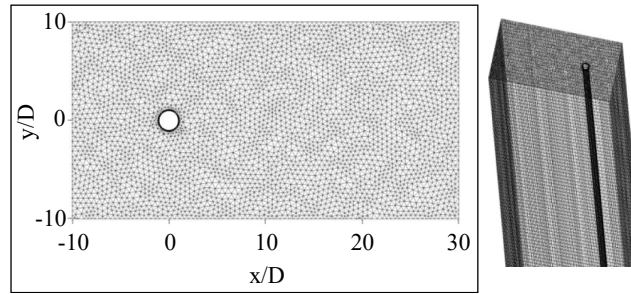
Fig. 2. Fluid mesh viewed from top (left) and the upper part of the 3D mesh (right), showing element length in the z-direction.
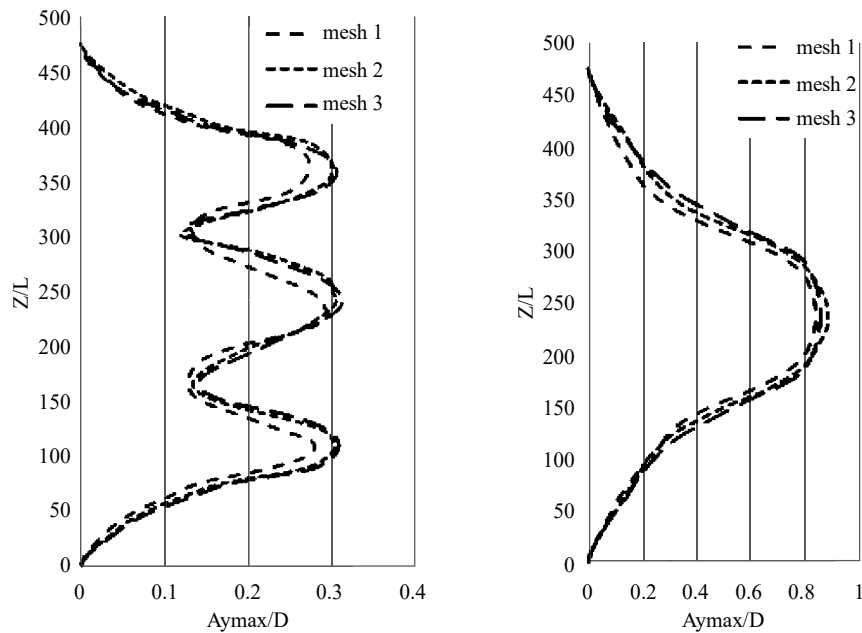
Fig. 3. Maximum riser oscillation in the IL (left) and CF (right) directions for the three analyzed meshes.

Coming back to eq. 8a and b, a finite element method must be used to discretise Eq. 8 and obtain the governing equation in the following form:

$$[M]\{\ddot{x}\}+[C]\{\dot{x}\}+[K]\{x\}=\{F\} \tag{14}$$

Where $\{x\}$ is the nodal moved distance in the three space dimensions $\{x, y, z\}$, $\{\dot{x}\}$ is the nodal velocity vector and $\{\ddot{x}\}$ the nodal acceleration vector. [M], [C] and [K] are the mass, damping and stiffness matrices, respectively. [F] is the hydrodynamic force vector. The governing equation is solved using the Hilber-Hughes-Taylor (HHT) method.

Next, a two-way explicit approach is utilized in the present FSI simulation, i.e., the fluid and solid equations are solved separately, and there are no iterations between the fluid and solid fields within one time step. Within a single time step, the flow equations are solved to obtain the forces on the riser. Then the forces are interpolated to the structural mesh using the conservative interpolation, and the structural dynamic equation is solved to obtain the quantities of riser motion.

After that, the displacements are interpolated to the fluid mesh with the profile preserving interpolation, and the positions of the mesh points are calculated and updated using the displacement diffusion model. The next time step begins with solving the flow equations in the updated mesh.

III. DESCRIPTION OF THE PROBLEM

This numerical approach is used to check the occurrence of lock-in for three different uniform flow velocities: 0.6 m/s (Re = 42K), 1.2 m/s (Re = 84K) and 1.8 m/s (Re = 126K). The Reynolds number is defined as: $Re = \rho VD / \mu$, where ρ is the water density, V the flow bulk velocity, D is the riser diameter and μ the water dynamic viscosity. During the synchronization analysis, a clarification of the riser pre-tension and total tension is included, total tension being the sum of the pre-tension and the hydrodynamic-induced-tension.

The model riser has a length to diameter ratio L/D = 475, mass ratio of $m = 0.937$, Young's modulus $E = 3.46e+10$ N/m^2 and inertia moment $I = 2.01e-6$ m^4. The structural damping is
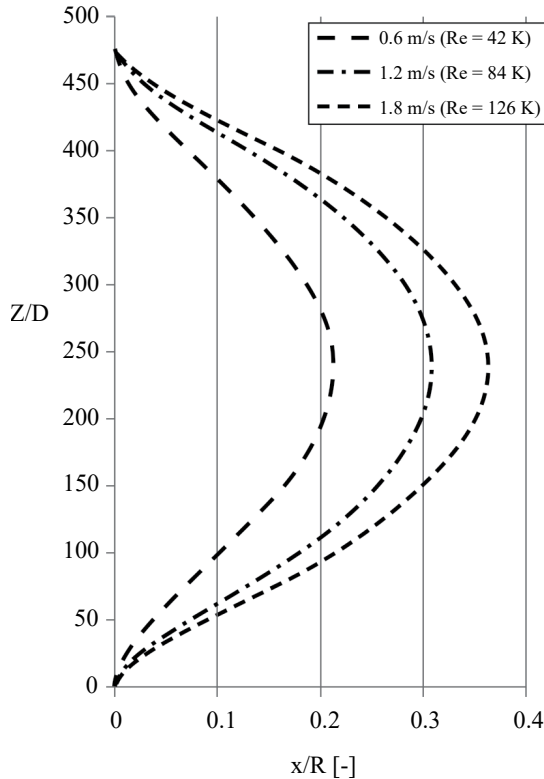
Fig. 4. Time-averaged dimensionless IL displacement for the three different Reynolds numbers.

set to zero, as is usual in a computational approach. The model´s configuration is shown in Fig. 1. The flow direction is the x-axis. The riser is fixed at both ends, and it is free to move in the x-direction, in-line movement (IL), and in the y-direction, cross flow movement (CF). No pre-tension is applied to the riser. The riser tension field will exclusively be the result of the riser response to the fluid forces.

The riser scheme shows its diameter D and length L as well as its coordinate reference system. The scheme of the riser within the fluid domain shows the domain dimensions: the domain length is 40D, and the domain width is 20D. The riser is located at a length from the inlet of 10D, and at same distance from the domain´s lateral sides, also 10D. The scheme shows also how the in-line flow direction (IL) denoted by the arrow of flow velocity V, corresponds with the x-axis; the riser length with the z-direction; and the cross-flow direction (CF) with the y-axis.

The fluid grid can be seen in fig. 2. It has a dense prism boundary layer, resulting from a mesh sensitiveness analysis. This was carried out in order to find the prism first layer thickness required to obtain both a value of $y^+ < 1$ for the maximum simulated velocity, 1.8 m/s, and a riser drag coefficient value near that of a cylinder, generally taken to be 0.65. It also has a good vortex shedding pattern. The final y^+ was lower than 1 and the C_D value obtained was 0.67. Therefore, the boundary layer was finally fixed to be 10 layers of prisms with an exponential growth of 1.35 and a first layer thickness

of 2e-5 m. In Fig. 2 (right) the vertical length of the elements, required to obtain accurate riser vibration mode shapes, can also be observed.

Following the recommendations of Holmes et al. (2006), the mesh of the riser has about 2.5K nodes on planes Z = 0 and Z = 475, concretely 2553. On the other hand, following the procedure of Xiao and Wang (2016) this number of elements by plane is kept and the z-length is divided into 200, 175 and 150 elements of equal length, to produce meshes 1, 2 and 3, respectively.

Afterward, a mesh sensitiveness analysis was carried out in order to check other possible sources of error, such as numerical diffusion or flow pressure mapping accuracy on the riser surface. The results can be observed in fig. 3, where the oscillation in both the IL and CF directions were recorded over time until maximum amplitude was reached. Mesh 2 was chosen for the simulations.

Time step analysis was carried out in the following way: knowing the anticipated frequency values, an initial estimation of the time step required to capture a wavelength with enough points was made. The first chosen time-step was 0.02 seconds, but simulations showed the need to reduce it. Values of 0.015 s and 0.0125 s were analyzed. The value of 0.015 seconds was acceptable for Reynolds numbers 42K and 84K, and 0.0125 s was found to be acceptable for Reynolds number 126K.

IV. RESULTS AND DISCUSSION

Fig. 4 shows the IL average dimensionless displacement from the original straight riser as function of the riser dimensionless length coordinate Z/D for the three shown current velocity values. The average deformation is an effect of the flow constant drag force, and from this average deformation shape the oscillation produced by oscillating vortex shedding forces takes place. The deformation is made dimensionless by dividing deformation by riser radius. Once obtained these deformation curves, their length is calculated as:

By applying equation 13 on the in-line average displacement curves of fig. 4 the riser length elongations *ΔL* are yielded. Entering these elongations and riser characteristics into equation 9 the riser tensions are obtained. Both elongations and tensions are shown in Table 2.

Finally, entering the riser material Young modulus *E,* the moment of inertia *I,* the mass per unit length and tension *T* into equations 10 to 12, the structural frequency spectrum is obtained, as shown in Table 3. Note that as tension varies with Reynolds number, and the tensioned-string frequency component depends on the tension, for each Reynolds number and associated tension there is a different set of tensioned-string frequency values.

As observed in Table 3, the frequency of the riser as a beam $f_{n,beam}$ is about one order of magnitude lower, having a negligible effect on the total frequency.

Table 4. Oscillation periods and frequency values for IL and CF oscillation as functions of Reynolds numbers.

Reynolds number	IL		CF	
	Z/D = 125	Z/D = 237.5	Z/D = 125	Z/D = 237.5
42K	0.360 s (2.78 Hz)	0.375 s (2.67 Hz)	0.735 s (1.36 Hz)	0.776 s (1.29 Hz)
84K	0.173 s (5.78 Hz)	0.171 s (5.85 Hz)	0.341 s (2.93 Hz)	0.348 s (2.88 Hz)
126K	0.146 s (6.84 Hz)	0.146 s (6.84 Hz)	0.292 s (3.42 Hz)	0.292 s (3.43 Hz)

1. Riser envelopes

In fig. 5 the IL oscillation (left) and CF lateral oscillation (right) for the three analyzed cases are shown. Vibration mode might increase with Reynolds number, as occurs when the Reynolds number changes from 42K to 84K, or it might remain the same, as occurs when the Reynolds number changes from 84K to 126 K. In the first case the oscillation mode changes from a 3rd mode to a 5th mode for the IL oscillation, and from a 1st mode to a 3rd mode for the CF oscillation.

CF maximum amplitude increases with Reynolds number, being about 0.7D for Re = 42K, just under 1.0D for Re = 84K and just under 1.5D for Re = 126K. This behavior agrees with observations made by Bourghet et al. (2011a), Resvanis et al. (2012), Xiao and Wang (2016) and others. The CF maximum amplitude is about three times the IL maximum amplitude, in agreement with results reported by Bearman (2011).

IL maximum amplitudes do not increase evenly. In fact, from Re = 42K to Re = 84K they decrease slightly. This might be the result from the increase in riser tension level that would make a greater turbulent force component in the flow direction necessary to produce the same oscillation.

The values of the IL oscillation amplitude at the envelope nodes are different from zero. The envelope nodes are the envelope span points with narrow amplitudes. This emphasizes the modulation of the standing wave pattern, which would have node widths of zero, by superimposing traveling wave components.

All the CF and IL responses are quite symmetric, but the IL oscillation for Re = 126K shows clear non-symmetric behavior. This has been observed also by Xiao and Wang (2016) and seems to be the oscillation instability before change to a higher oscillation mode for Reynolds numbers immediately higher.

2. Oscillation time histories

In fig. 6 the oscillation time histories for both IL (left) and CF movements (right) are shown. In all cases the time to reach a stable pattern has been subtracted. It can be observed how, for all three cases, the IL response frequency is nearly twice that of the CF response frequency as Table 4 shows. It can be also observed that the procedure accuracy is good, being the frequency value difference between predictions (Table 3) and results (Table 4) small, and a result of water damping, as it was also observed by Huang et al. (2011b). Also, just as observed by authors such as Resvanis et al. (2012) and Xiao and Wang (2016), the IL and CF oscillation frequencies increase with the Reynolds number.

This implies that, as the IL frequency is nearly twice the CF frequency, the riser behaves as a tensioned string, Lie and Kaasen (2006). This demonstrates that the riser is a tensioned riser even if it is not pre-tensioned. Rather, it is tensioned by the effect of the fluid flow. For a non-tensioned beam the ratio is lower than 2, due to the quadratic relationship between mode and frequency, eq. 12 and 13, Weaver et al. (1974).

In fig. 6 it can also be observed that CF oscillation is not always shown as being formed by perfectly shaped sinusoidal shapes, while on the other hand, IL oscillation is. This non-sinusoidal shape is more intense in the Z/D = 125 riser span than in the Z/D = 237.5 one. The explanation of this effect, also observed in some oscillation time histories by Xiao and Wang (2016), is the presence of harmonics of slightly different frequencies and smaller amplitudes.

3. Synchronization analysis

Now, the synchronization or lock-in phenomenon is analyzed for the three Reynolds number cases. In fig. 7 the riser CF lateral oscillation at the two displayed riser sections is shown again on the left side. The transversal component of the flow velocity at a point downstream of the riser and at the same riser spanwise point can be seen on the right side. The comparison of frequency values for both the CF riser oscillation and the transversal velocity component as a means of quantifying the vortex shedding frequency is the method to analyze synchronization, Bourghet et al. (2011a). The line where this transversal velocity component is measured is located downstream of the riser at $(x, y) = (15D, 0)$. For the same riser spanwise values Z/D = 125 and 237.5 on this line, a sample point appears where the CF component of the velocity is measured across time.

For the Reynolds number 42K case the results show that the periods between curve nodes--that is, where oscillation curves cross the y = 0 axis--for both the frequency of the transversal component of the flow velocity, and the frequency of CF vibrations, are 1.32 ± 0.005 Hz for both spanwise points. The other way to measure these frequency values is shown in fig. 8, which displays the CF oscillation and transversal velocity component results in the frequency domain instead of in the time domain. The frequency-domain results are obtained by applying the Fast Fourier Transform to the time-dependent results. The frequency value 1.32 Hz is again obtained. This frequency is lower than the natural frequency for such vibration modes, 1.67 Hz. This effect has also been found by other authors, Bourghet et al. (2011a, 2013).
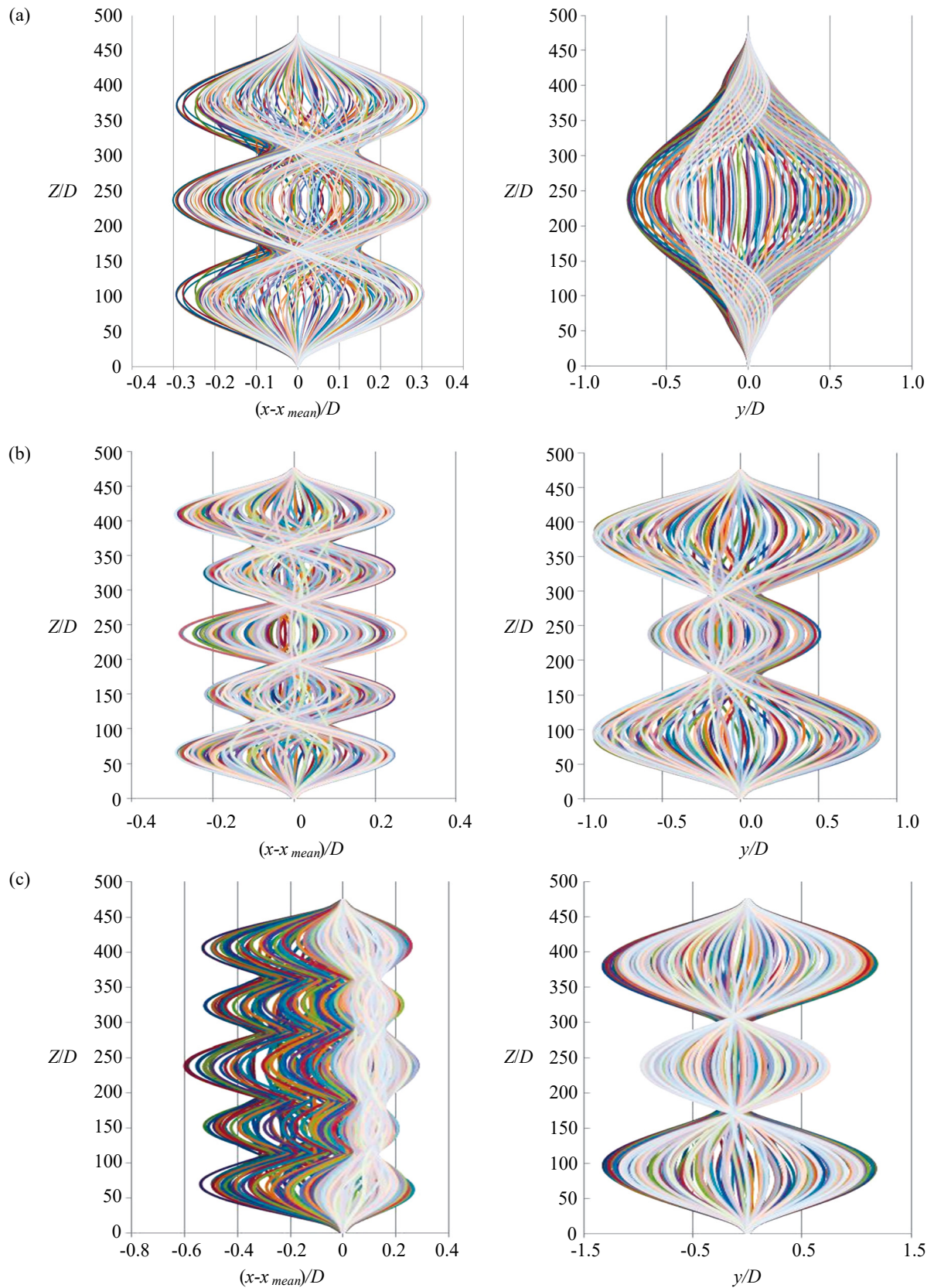
Fig. 5. Riser response IL envelope (left) and CF envelope (right) for the three Reynolds numbers: a) Re = 42K, b) Re = 84K and c) Re = 126K.
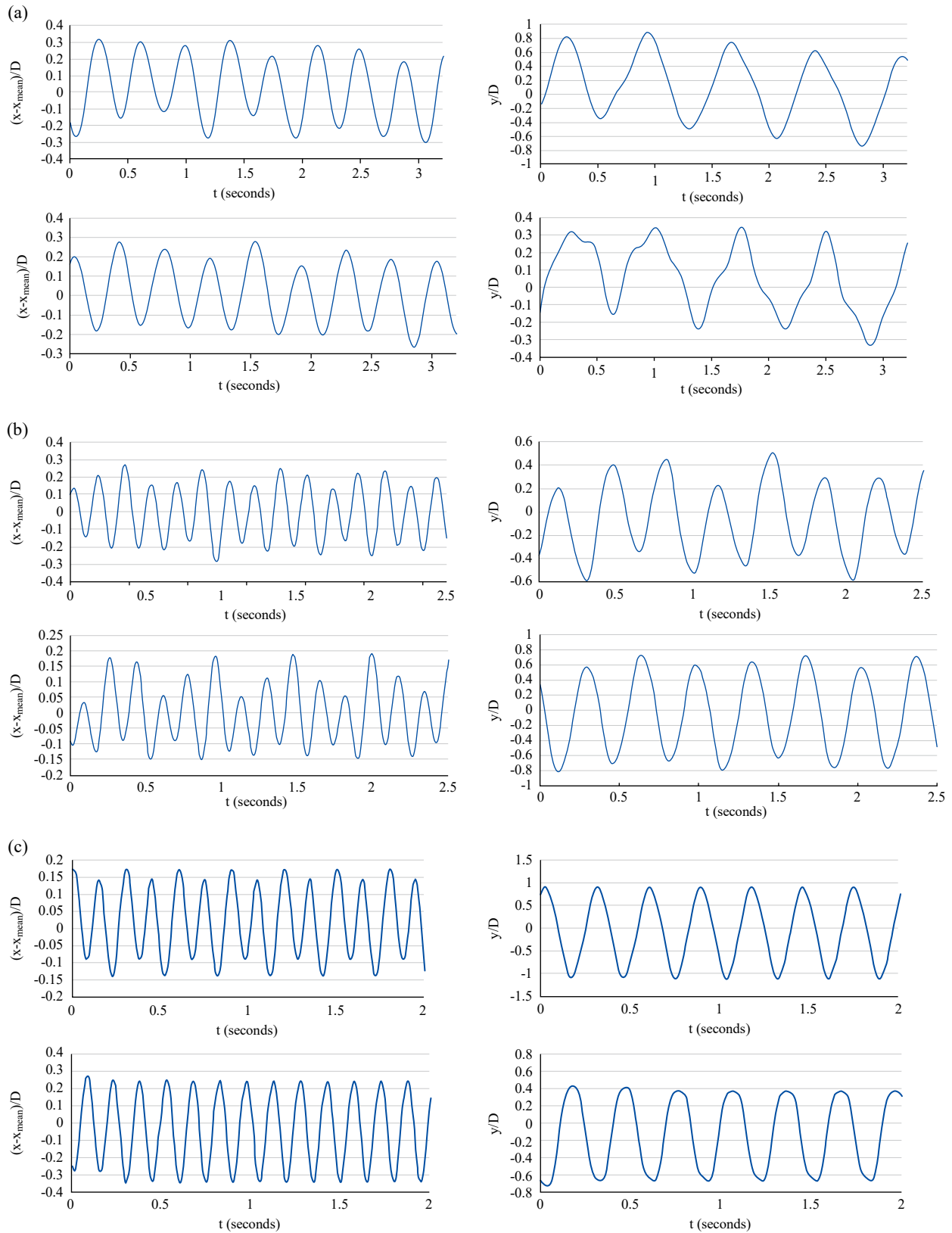
Fig. 6. Oscillation time histories at Z/D = 237.5 (upper) and Z/D = 125 (lower) showing IL oscillation (left) and CF oscillation (right) for the three Reynolds numbers: a) Re = 42K, b) Re = 84K and c) Re = 126K.
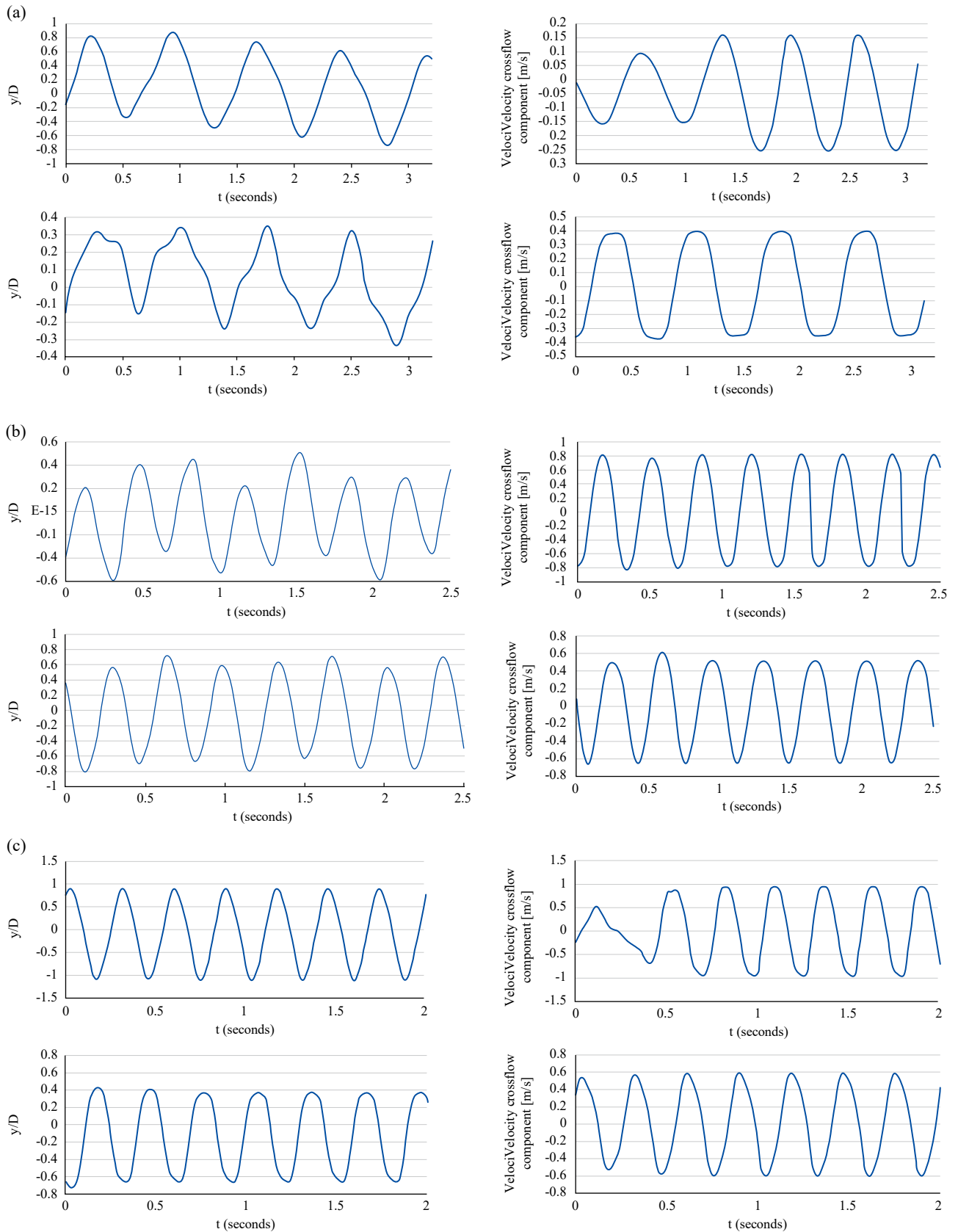
Fig. 7. Riser CF oscillation (left) and transversal flow velocity (right) for sections Z/D = 237.5 (upper) and Z/D = 125 (lower) and for the three Reynolds numbers: a) Re = 42K, b) Re = 84K and c) Re = 126K.
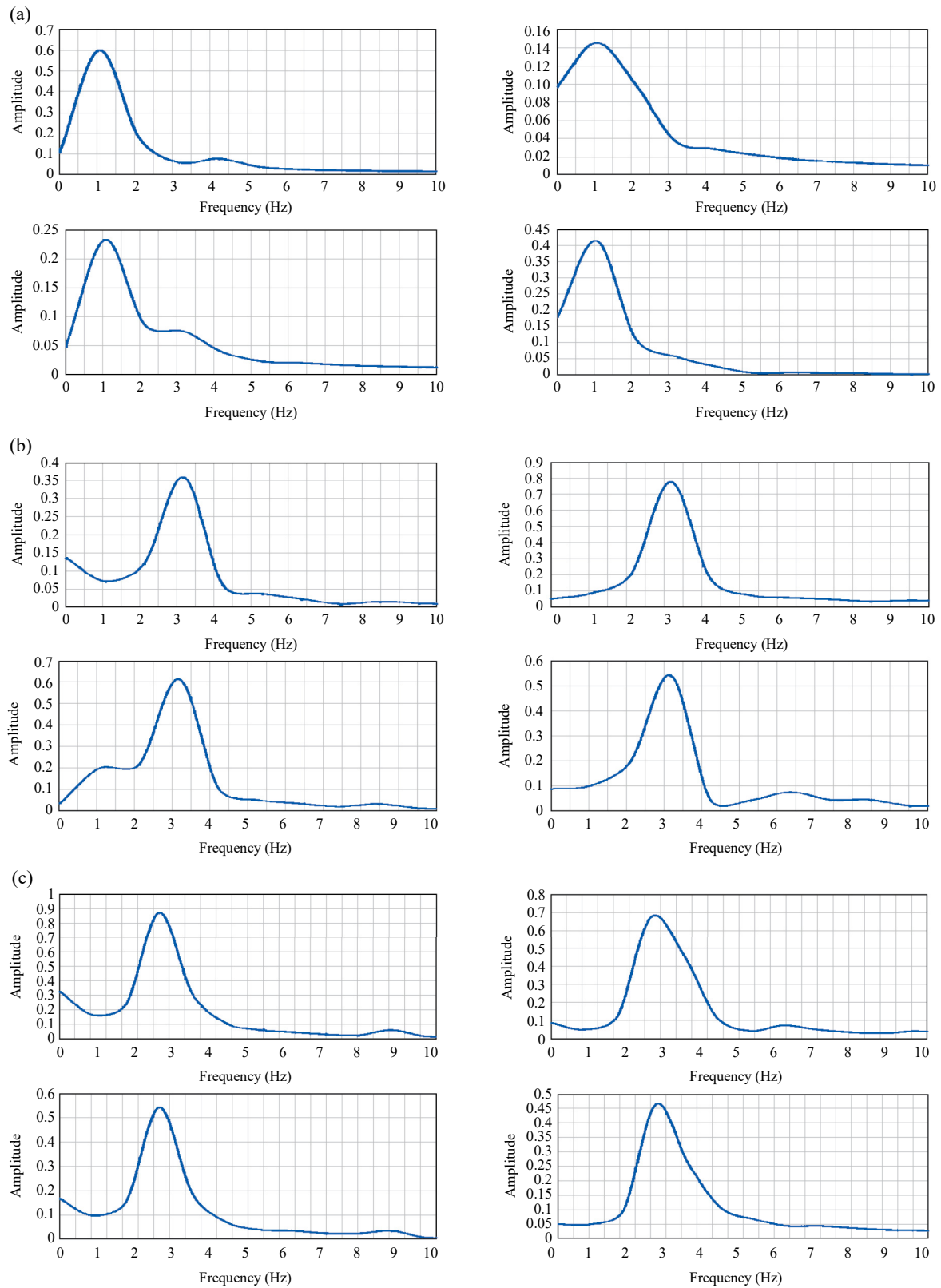
Fig. 8. Frequency spectra of the riser CF oscillation (left) and transversal flow velocity (right) for sections Z/D = 237.5 (upper) and Z/D = 125 (lower) and for the three Reynolds numbers: a) Re = 42K, b) Re = 84K and c) Re = 126K.
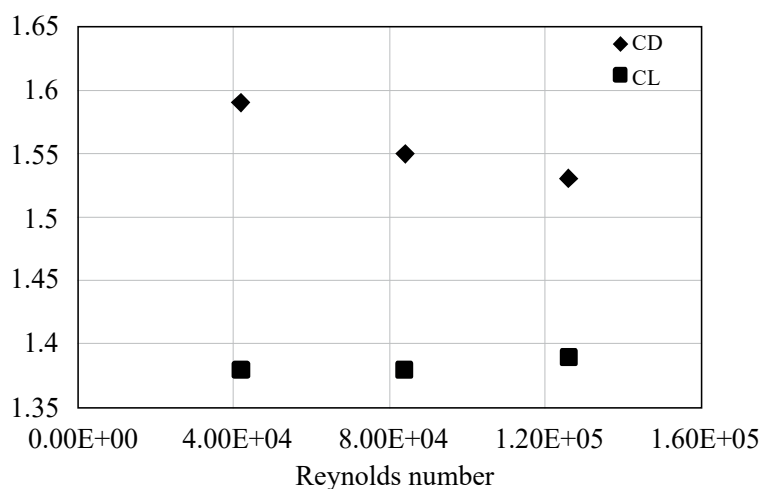
Fig. 9. Drag and lift force coefficients as functions of Reynolds numbers.

Fig. 8 also shows that the riser oscillation presents two peaks, one at the above main frequency, and a second one at about three times this frequency, and is of smaller amplitude. The transversal velocity spectrum shows only one frequency peak, the vortex shedding frequency. Lock-in takes place at the main frequency, as observed by Bourghet et al. (2011a). The difference in values between the CF oscillation and the transversal velocity component is small enough to be considered lock-in.

4. Fluid forces

In fig. 9 the drag and lift force coefficients, C_D and C_L are shown for the three analyzed cases. The drag force coefficient C_D shows a decreasing behavior when the Reynolds number increases, but in all cases is much larger than that of a fixed cylinder. This pattern was also observed by Resvanis et al. (2012). On the other hand, the lift force coefficient C_L remains quite stable when the Reynolds number increases, as it isslightly higher for the higher Reynolds number, Re = 126K. This behavior corresponds well with the observations of Bourghet et al. (2011a).

5. Orbital trajectories

Fig.10 shows the trajectories of different Z/D sections in their x – y planes. The forms that appear are typical of tensioned risers, and similar to those observed by Xiao and Wang (2016) with some differences due to the much higher Reynolds number range. These differences are, first, that both the IL and CF amplitudes are much larger. And second, that both the IL and CF oscillation amplitudes increase. Nevertheless, the IL amplitude increases in a particular way: as the Reynolds number grows the trajectory tends to "collapse" into a thicker curve. That is to say, as the Reynolds number increases, and for a certain CF position of the trajectory, the differences of IL amplitudes among the several oscillation periods are smaller. As an example, for Z/D = 50 the trajectory for Re = 84K is similar to a lemniscates, but when the Reynolds number in-

creases to Re = 126K the trajectory "collapses" to almost a half-circumference.

Also interesting is the fact that the "non-collapsed" trajectories move counterclockwise. According to Bourghet et al. (2011b), the counterclockwise direction is predominant in the synchronization region. Thus, this movement direction corresponds well with the equality of CF oscillation and transversal velocity frequency values found in the synchronization chapter. In the "collapsed" trajectories there is no room for clockwise or counterclockwise movements.

Comparing these results with the low Reynolds numbers ofXiao and Wang (2016), much bigger amplitudes in the CF direction can be observed, but in the IL direction the higher average deformation and tension produces a smaller amplitude, as the vortex shedding forces to average drag force ratio becomes smaller. The CF oscillation amplitude increases with the Reynolds number following the observations of the tests carried out for the same Reynolds number range by Resvanis et al. (2012)

V. CONCLUSIONS

The main results obtained in the present work are the following: the dominant mode numbers in the IL and CF oscillations either increase or remain the same as the Reynolds number increases. Before the change of vibration mode one vibration instability appears that is observed as a non-symmetric oscillation envelope. This occurs first in the IL direction.

Both the IL and CF oscillation average amplitudes increase with the Reynolds number. Nevertheless, locally the IL amplitude can decrease. This is because, for the IL oscillation, where vibration moves in the same direction as the flow, the riser is heavily tensioned in this direction, and the vortex shedding forces required to produce a wide oscillation are much higher.

Dominant frequencies and the lift coefficient also increase
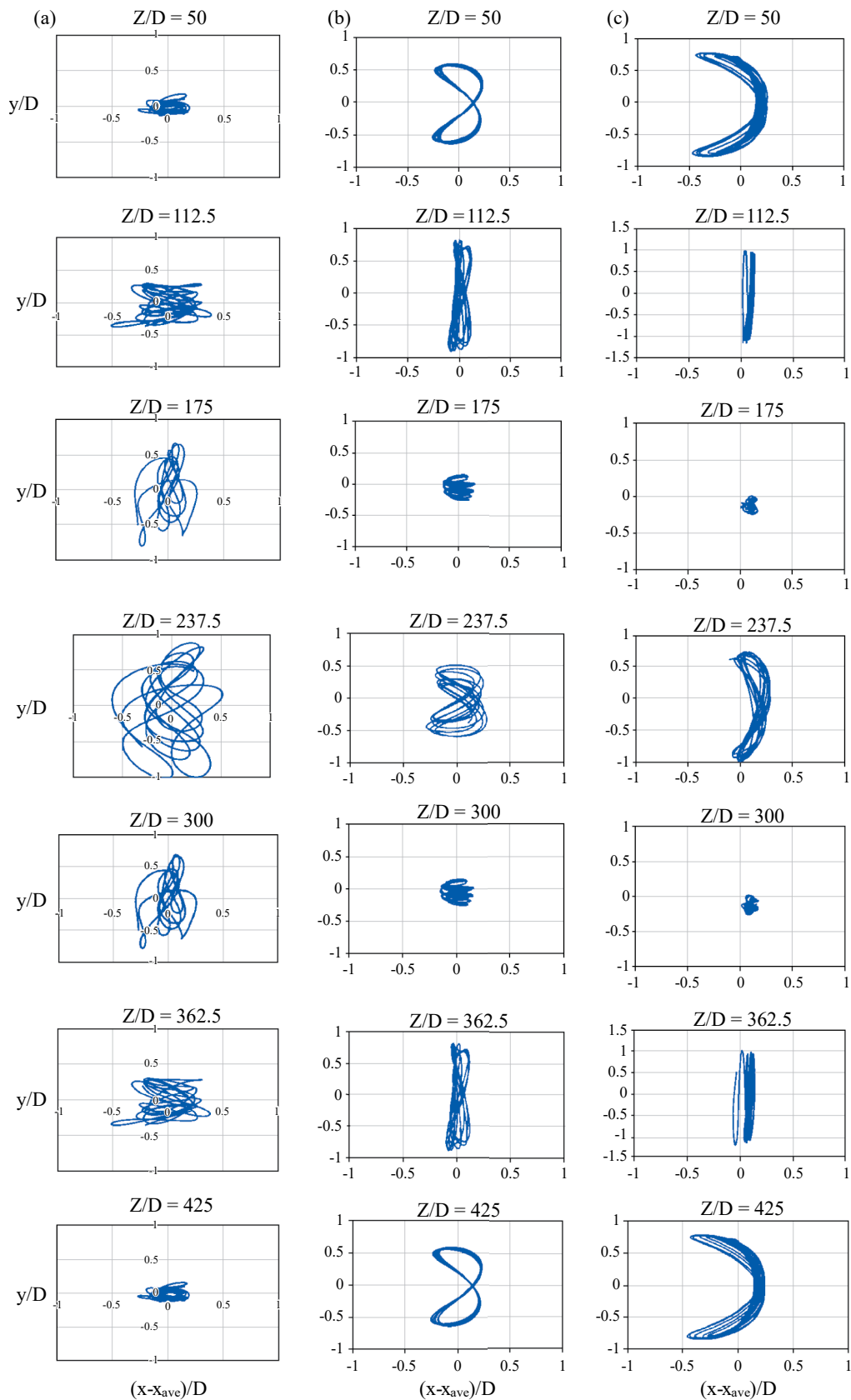
Fig. 10. Trajectories of different riser Z/D sections for a) Re = 42K, b) Re = 84K and c) Re = 126K.

with the Reynolds number, but the drag coefficient decreases.

The CF maximum amplitudes are about 3 times the IL maximum amplitudes, and as occurs with the IL maximum amplitude, it also increases with the Reynolds number.

Fluid forces can turn a riser into a tension-dominated riser even if the riser is not a pre-tensioned riser. The riser IL frequencies are nearly twice the CF frequencies. This implies that the riser behaves as a tension-dominated riser.

Including the flow-induced tension in the analytical calculation of the riser vibration frequencies allows much higher calculation accuracy.

Synchronization analysis has been performed by calculating and directly comparing the oscillation period in the CF oscillation time histories to the transversal component of the velocity. It has also been checked by calculating the frequency spectra of these variables in the frequency domain with the Fast Fourier Transform, and finally, by checking the counterclockwise movement of riser orbital trajectories. The lock-in condition is established at the vibration mode predominant frequency for the three Reynolds numbers.

REFERENCES

Bearman, P. W. (1984). Vortex shedding from oscillating bluff body. Annual Review of Fluid Mechanics 16, 195-222.

Bearman, P. W. (2011). Circular cylinder wakes and vortex-induced vibrations. Journal of Fluids Structures 27, 648-658.

Bourghet, R., G. E. Karniadakis and M. S. Triantafillou (2011a). Lock-in of the vortex-induced vibrations of a long tensioned beam in shear flow. Journal of Fluids Structures 838-847.

Bourghet, R., G. Modarres-Sadegui, G. E. Karniadakis and M. S. Triantafillou (2011b). Wake-body resonance of long flexible structures is dominated by counterclockwise orbits. Physics Review Letter 107 (134502), 1-4.

Bourghet, R., D. Lucor and M. S. Triantafillou (2012). Mono- and multi-frequency cortex-induced vibrations of a long tensioned beam in sheared flow. Journal of Fluids Structures 32, 52-64.

Bourghet, R., G. E. Karniadakis and M. S. Triantafillou (2013). Phasing mechanism between the in-line and cross-flow vortex-induced vibrations of a long tensioned beam in sheared flow. Computers and Structures 122, 155-163.

Bourghet, R., G. E. Karniadakis and M. S. Triantafillou (2015). On the validity of the independence principle applied to the vortex-induced vibrations of a flexible cylinder inclined at 60 degrees. Journal of Fluids Structures 53, 58-69.

Chaplin, J. R., P. W. Bearman, F. J. Huera-Huarte and R. J. Pattenden (2005). Laboratory measurement of vortex-induced vibrations of a vertical tension riser in a stepped current. Journal of Fluids Structures 21, 3-24.

Gabbai, R. D. and H. Benaroya (2005). An overview of modeling and experiments of vortex-induced vibrations of circular cylinders. Journal of Sound Vibration 282, 575-646.

Gao, Y., S. Fu, T. Ren, Y. Xiong and L. Song (2015). VIV response of along flexible riser fitted with strakes in uniform and linearly sheared currents. Applied Ocean Research 52, 102-114.

Govardhan, R. and C. H. K. Williamson (2006). Defining the modified Griffin plot in vortex-induced vibrations: revealing the effect of Reynolds number using controlled damping. Journal of Fluid Mechanics 561, 147-180.

Gu, J., M. Vitola, J. W. P. Coelho, M. Duan and C. Levi (2013). An experimental investigation by towing tank on VIV of a long flexible cylinder for deep water riser applications. Journal of Marine Science and Technology 18, 358-369.

Holmes, S., Y. Constantinides and O. H. Oakley, Jr. (2006). Simulation of riser VIV using fully three dimensional CFD simulations, OMAE2006-92124.

Proceedings of the ASME 25th International Conference on Ocean, Offshore and Arctic Engineering, Hamburg, Germany.

Huang, K., H. C. Chen and C. R. Chen (2011a). Numerical scheme for riser motion calculation during 3D VIV simulation. Journal of Fluids Structures 27, 947-961.

Huang, S., M. Khorasanchi and K. Hertfjord (2011b). Drag amplification of long flexible riser models undergoing multi-mode VIV in uniform currents. Journal of Fluids Structures 27, 342-353.

Jhingran, V., J. Jaiswal and J. K. Vandiver (2008). Spatial variation of drag on long cylinders in sheared flow. OMAE2008-57803. Proceedings of the ASME 27TH International Conference on Ocean, Offshore and Arctic Engineering. Estoril, Portugal.

Khalak, A. and C. H. K. Williamson (1999). Motions, forces and mode transitions in vortex-induced vibrations at low mass-damping. Journal of Fluids Structures 13, 813-851.

Lie, H. and K. E. Kaasen (2006). Modal analysis of measurements from a large-scale VIV model test of a riser in linearly sheared flow. Journal of Fluids Structures 22 557-575.

Lothode, C., G. Fontaine, E. Guilmineau, A. Wang, F. Vertallier, M. Minguez, A. Cinello and D. Gross (2015). Numerical study of VIV over a flexible riser. VI International Conference on Computational Methods in Marine Engineering, MARINE 2015. Roma, Italy.

Meneguini, J. R., F. Saltara, C. T. Yamamoto, E. Casaprima and J. A. Ferrari (2004). Numerical simulation of VIV on long flexible cylinders immersed in complex flow fields. European Journal of Mechanics B/Fluids 23, 51-63.

Menter, F. R. (1994). Two equation eddy-viscosity turbulence models for engineering applications. American Institute of Aeronautics and Astronautics Journal 32 (8), 1598-1605.

Menter, F. R., P. Sharkley, S. Yakubov and M. Kuntz (2006). Overview of fluid-structure coupling in ANSYS-CFX, OMAE2006-92145. Proceedings of the ASME 25th International Conference on Ocean, Offshore and Arctic Engineering, Hamburg, Germany.

Newman, D. J. and G. E. Karniadakis (1997). A direct numerical simulation study of flow past a freely vibrating cable. Journal of Fluid Mechanics 344, 95-136.

Resvanis, T. L., V. Jhingran, J. K. Vandiver and S. Liapis (2012). Reynolds number effects on the vortex-induced vibration of flexible marine risers. OMAE2012-83565. Proceedings of the ASME 31st International Conference on Ocean, Offshore and Arctic Engineering. Rio de Janeiro, Brazil.

Sarpkaya, T. (1979). Vortex-induced oscillations. Journal of Applied Mechanics 46, 241-248.

Tognarelli, M. A., S. T. Slocum, W. R. Frank and R. B. Campbell (2004). VIV response of a long flexible cylinder in uniform and linearly sheared currents, OTC 16338. Proceedings of the 2004 Offshore Technology Conference. Houston, USA.

Tognarelli, M. A., S. Taggart and M. Campbell (2008). Actual VIV fatigue response of full scale drilling risers: with and without suppression devices. OMAE2008-57046. Proceedings of the ASME 27th International Conference on Ocean, Offshore and Arctic Engineering. Estoril, Portugal.

Trim, A. D., H. Braaten, H. Lie and M. A. Tognarelli (2005). Experimental investigation of vortex-induced vibration of long marine risers. Journal of Fluids Structures 21, 335-361.

Vandiver, J. K., S. Swithenbank, V. Jaiswal and H. Marcollo (2006). The effectiveness of helical strakes in the suppression of high-mode number VIV, OTC 18276. Proceedings of the 2006 Offshore Technology Conference. Houston, USA.

Vandiver, J. K., V. Jaiswal and and V. Jhingran (2009). Insights on vortex-induced, traveling waves on long risers. Journal of Fluids Structures 25, 641-653.

Weaver, W., S. P. Timoshenko and D. H. Young (1974). Vibration Problems in Engineering. John Wiley & Sons, New York, USA.

Williamson, C. H. K. and R. Govardhan (2004). Vortex-induced vibrations. Annual Review of Fluid Mechanics 36, 413-455.

Wu, X., F. Ge and Y. Hong (2012). A review of recent studies on vor-

tex-induced vibrations of long slender cylinders. Journal of Fluids Structures 28, 292-308.

Xiao, Q. and E. Wang (2016). Numerical simulation of vortex-induced vibration of a vertical riser in uniform and linearly sheared currents. Ocean Engineering 121, 492-515.

Xue, H., K. Wang and W. Tang (2015). A practical approach to predicting cross-flow and in-line VIV response for deepwater risers. Applied Ocean Research 52, 92-101.